Journal of Solid State Chemistry 182 (2009) 2678–2684

Contents lists available at ScienceDirect

Journal of Solid State Chemistry

journal homepage: www.elsevier.com/locate/jssc

Electronic band structure of $CaUO_4$ from first principles

S.F. Matar *, G. Demazeau

CNRS, Université de Bordeaux, ICMCB, Centre de Ressources Hautes Pressions, 87 avenue du Docteur Albert Schweitzer, F-33608 Pessac Cedex, France

ARTICLE INFO

Article history:
Received 7 May 2009
Received in revised form
6 July 2009
Accepted 12 July 2009
Available online 21 July 2009

Keywords:
Uranium oxide
DFT
VASP
ASW
ELF

ABSTRACT

Band theoretical results are presented on calcium uranate, $CaUO_4$, based on computations within the density functional theory. From pseudo-potential calculations the equation of state is obtained with equilibrium lattice properties in agreement with experiment. For isotropic volume change the bulk modulus amounts to 180 GPa but a much higher value is found for anisotropic compression along the hexagonal *c*-axis. This is assigned to the short U–O distances in linear uranyl polycation. Scalar relativistic all-electron calculations point to a semiconductor with ~3 eV band gap. From density of states, chemical bonding and electron localization function ELF, oxygen is found to behave both as ionic and covalent in the coordination sphere of uranium. The results provide an illustration of the peculiar role of uranyl cation UO_2^{2+} according to its chemical environment.

1. Introduction

Uranyl cation, UO_2^{2+}, is found in several chemical systems such as the halides UO_2X_2 (X = F, Cl) [1,2] and the oxides AUO_4 (A = Ca, Sr, Ba, Pb, Cd) which can then be formulated as: $A(UO_2)O_2$ [3]. Most of these compounds were synthesized and studied by X-ray diffraction in the first half of last century, mainly during the investigation of uranium compounds for strategic purposes. For such technologically relevant systems, establishing the equation of state (EOS) and accessing the electron band structure as well as the properties of chemical bonding are needed both at the fundamental and application levels. For the latter this may involve a better mastering of the handling and disposal of the chemical products when they occur as secondary waste in nuclear reactors for instance. In this context we mention a recent theoretical work on uranyl peroxides [4]. The studies can be accurately carried out within the well established density functional theory DFT [5,6] quantum mechanics framework which provides reliable energy derived quantities. While such investigations have been undertaken for UO_2 [7,8], UF_6 [9] as well as recently discussed band structure of UO_2F_2 [10], no band theoretical results are known for the uranate systems. For the purpose of investigating the electronic and chemical bonding properties of uranyl polycation in uranate AUO_4 systems, we here study the Ca member. It is isostructural and isoelectronic (32 valence electrons) of UO_2F_2, so that comparisons will be enabled especially as to the changes of its chemical environment from fluorinated to oxygenated ones.

Two complementary methods built within DFT were used. Firstly with pseudo-potential methodology a full geometry optimization is carried out to obtain the equation of state (EOS) and related equilibrium quantities for the energy, the bulk modulus and volume. Then with all-electron calculations, the electronic band structure and the chemical bonding properties are assessed.

2. Computational framework

Within DFT, calculations of the EOS and electron localization were carried out using a pseudo-potential (PP) approach with the Vienna ab initio simulation package (VASP) code [11]. Projector augmented wave (PAW) [12,13] potentials built within the local density approximation (LDA) [14] as well as the generalized gradient approximation (GGA) [15] were used. Besides of being much more accurate than ultra-soft PP's, PAW potentials treat the *f* orbitals as valence states. The optimization of the structural parameters is performed until the forces on the atoms are less than 0.02 eV/Å and all stress components are below 0.003 eV/Å^3. Calculations are converged at an energy cut-off of 500 eV for the plane-wave basis set. Brillouin zone (BZ) integrals are approximated [16] using **k**-point grids with a starting mesh of $4 \times 4 \times 4$ up to $8 \times 8 \times 8$ for best convergence and relaxation to zero strains. Further, from the calculations a mapping of the electrons in the lattice can be obtained using the electron localization function (ELF) scheme, introduced by Becke and Edgecombe [17]. It allows determining the amount of localization of electrons with respect to the free electron gas distribution. The dimensionless ELF magnitude ranges from 0 to 1 with ELF $= \frac{1}{2}$ corresponding to the

* Corresponding author. Fax: +33 540002761.
E-mail address: matar@icmcb-bordeaux.cnrs.fr (S.F. Matar).

0022-4596/$ - see front matter © 2009 Elsevier Inc. All rights reserved.
doi:10.1016/j.jssc.2009.07.023

free electron gas distribution. These three extreme situations will be illustrated by three sets of colors: ELF = 0 points to no localization (blue contours), ELF = 1 points to strong localization (red contours) and ELF = $\frac{1}{2}$ with green contours. The latter are most likely observed for metallic systems.

All-electron calculations, necessary to explore the whole valence band (VB)/conduction band (CB) spectrum, were performed using the scalar-relativistic implementation of the augmented spherical wave (ASW) method [19,20] based on the DFT. As it was established from the PP calculations that the GGA provided the correct ground state (cf. next section), the computations used GGA scheme [15]. In the ASW method, the wave function is expanded in atom-centered augmented spherical waves, which are Hankel functions and numerical solutions of Schrödinger's equation, respectively, outside and inside the so-called augmentation spheres. In the minimal ASW basis set, we chose the outermost shells to represent the valence states and the matrix elements were constructed using partial waves up to $l_{max.}+1=4$ for U including 5*f* sub-shell and $l_{max.}+1=2$ for Ca and O. The ASW method uses the atomic sphere approximation (ASA) which assumes overlapping spheres centered on the atomic sites whose volume is equal to the cell volume. In order to represent the correct shape of the crystal potential in the large voids of the crystal structure (Fig. 1), additional augmentation spheres were inserted to avoid an otherwise too large overlap between the actual atomic spheres. These are called empty spheres (ES) described as pseudo-atoms with zero atomic number and basis set $l_{max.}+1=2$ up to 3, allowing them to receive charges from the neighboring atomic species. The choice of these sites as well as the augmentation radii are automatically determined using the sphere-geometry optimization algorithm [21]. All calculations are started for neutral atom configurations. Convergence is obtained when negligible variations for the charges ($\Delta Q=10^{-8}$) and for the total energy ($\Delta E=10^{-7}$ eV), are observed between two successive iterative cycles. Self-consistency was achieved by a highly efficient algorithm for convergence acceleration [22]. The BZ integrations were performed using the linear tetrahedron method with up to 280 **k**-points generated from 2744 points in the irreducible wedge [12,20]. Information about the nature of the chemical bond between two atomic constituents (*i*,*j*) is qualitatively discussed from the "covalent bond energy" (ECOV) criterion [23] criterion which combines overlap (S_{ij}) [24] and Hamiltonian (H_{ij}) [25] populations. Besides ECOV we also show the integrated quantities (*i* ECOV) allowing examination of the relative strengths of the bonds. In the plots, negative, positive and zero magnitudes are indicative of bonding, antibonding, and nonbonding interactions respectively.

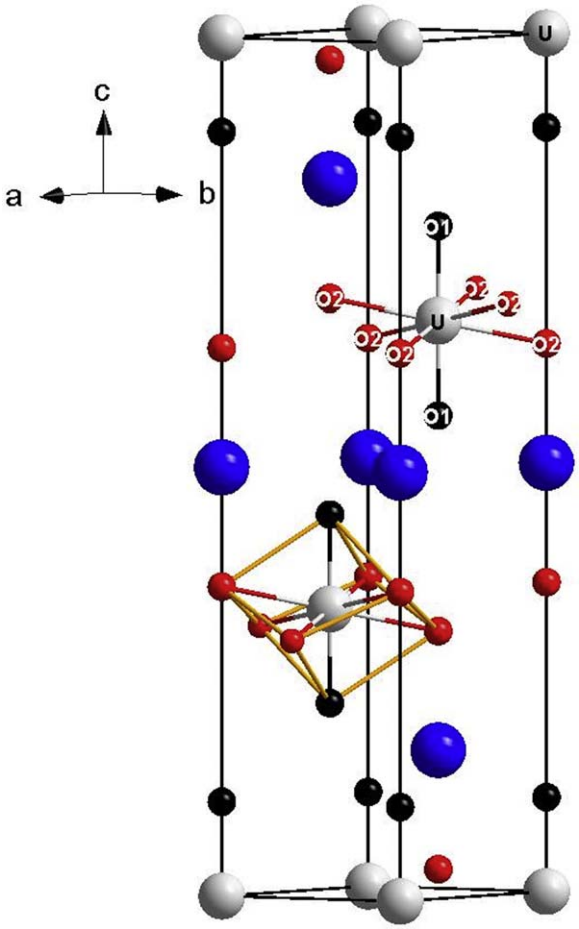

Fig. 1. Crystal structure of $CaUO_4$ with hexagonal axes. Large (blue) spheres represent Ca. The UO_8 polyhedron is sketched in lower part (cf. text for more details). (For interpretation of the references to colour in this figure legend, the reader is referred to the web version of this article.)

3. Geometry optimization from pseudo-potential calculations

3.1. Crystal structure considerations

The crystal structure of $CaUO_4$ is rhombohedral ($R\bar{3}m$ space group, ♯166) with 1 formula unit (f.u.) per cell [3]. It can be considered as a deviation from double CaF_2 fluorite structure viewed in rhombohedral symmetry. The experimental lattice parameters are given in Table 1. For a clear representation the structure can be described with hexagonal axes with a cell containing 3 f.u. as shown in Fig. 1. Uranium is surrounded with two types of oxygen atoms, respectively with two and six coordinations: the apical ones, along the *c*-axis, are labeled as O1 and the equatorial ones are designated as O2. Note that in isostructural uranyl fluoride the latter are replaced by F—cf. Table 1—and calcium is inserted in the Van der Waals gaps between the UO_2X_6 entities, X = O, F.

For the sake of better discussing the forecoming computational results we consider an alternative description of uranium environment. This can be viewed starting from the eightfold

Table 1
Lattice parameters of $CaUO_4$ and related systems with $R\bar{3}m$ space group, ♯ 166.

System	rh-$Ca_2F_4^{\dagger}$	UO_2F_2 [2]	$CaUO_4$ [3]	$CaUO_4^{\dagger}$
a-Latt. const. (Å)	6.418	5.764	6.254	6.210
α	34°62'	42°43'	36°2'	36°07'
Atoms				
1*a* (0,0,0)	Ca1	U	U	U
1*b* ($\frac{1}{2},\frac{1}{2},\frac{1}{2}$)	Ca2	–	Ca	Ca
2*c* ±(*u*, *u*, *u*)	F1, u = 0.126	O, u = 0.122	O1, u = 0.109	O1, u = 0.113
2*c* ±(*v*, *v*, *v*)	F2, v = 0.374	F, v = 0.294	O2, v = 0.361	O2, v = 0.363
Distances (Å)				
	Ca1−F1 = 2.29	U−O = 1.74	U−O1 = 1.94	U−O1 = 1.98
	Ca1−F2 = 2.31	U−F = 2.43	U−O2 = 2.30	U−O2 = 2.31
	Ca2−F2 = 2.29		Ca−O1 = 2.43	Ca−O1 = 2.42
	Ca2−F1 = 2.31		Ca−O2 = 2.38	Ca−O2 = 2.33
Volume (Å^3)	75.7	79.4	76.1	75.2
$B_0^{iso.}$ (GPa)	80	150 [10]		180
$B_0^{aniso.}$ (GPa)	100	590 [10]		410

Results with † symbol are from present investigations. Note the relationship Rhomhedral–Hexagonal for lattice parameters: $a_H=a_R\sqrt{2(1-\cos\alpha)}$ and $c_H=a_R\sqrt{3(1+2\cos\alpha)}$.

coordinated calcium in fluorite CaF_2 ($Fm\bar{3}m$ space group, #225). In the CaF_8 cube the eight Ca–F distances are equal (cf. Table 1). Replacing Ca by U and 2 F by 2 O along the cube diagonal gives a UO_2F_6 polyhedron observed in UO_2F_2. Within $CaUO_4$, two O1 along cube diagonal and six O2 for remaining oxygen give a less distorted polyhedron than in the fluoride. The $d_{U-O1}/d_{U-O2} = 0.83$ ratio is larger than in the fluoride: $d_{U-F}/d_{U-O} = 0.72$, so that the uranyl polycation may be considered as "smaller" in the latter. These features will be shown to have consequences on the physico-chemical properties.

3.2. Structure optimization

Starting from the experimental setup of $CaUO_4$ in Table 1, a full geometry relaxation was carried out with PAW potentials constructed with LDA and GGA exchange-correlation functionals for a search of the correct structure in comparison with experiment. At energy convergence and minimum lattice strains, the GGA-PAW calculations led to better agreement of the cell volumes for both oxides than LDA-PAW which gives smaller values. Then the calculational results in this paper are based on the GGA gradient exchange-correlation functional. Nevertheless, GGA + U calculations (U: Coulomb repulsion parameter allowing to enhance correlation) were tested for completeness. From last column of Table 1 giving the relaxed lattice parameters, an overall agreement with experiment is found. This also stands for the oxygen internal coordinates which give distances in the same trend as experiment.

Further in view of the crystal structure description an additional calculation was started for rhombohedral fluorite, rh-Ca_2F_4 with the lattice constants of $CaUO_4$ by replacing U by another Ca and oxygen by fluorine. The resulting fully relaxed geometry is found in the same rhombohedral starting symmetry. The results in Table 1 show that the internal coordinates of F give two sets of close Ca–F distances: two apical with 2.29 Å and six equatorial with 2.31 Å. These values are smaller but close to the Ca–F distance of 2.36 Å in cubic CaF_2. The cell volume of 75.7 $Å^3$, i.e. $V = 37.85$ $Å^3$ per f.u. is also close to the experimental volume per f.u. which amounts to 40.69 $Å^3$ (note that $Z = 4$ f.u. in face centered lattices). Then our relaxed rhombohedral structure for CaF_2 describes fairly well the experiment and should allow establishing comparisons with actual case study of calcium uranate.

3.3. Electron localization mapping

An illustration of the results is further obtained from the electron localization function, ELF. The plot for a vertical plane along the hexagonal *c*-axis crossing all species is given in Fig. 2. The linear "O1–U–O1" entities are observed with strong localization around them (red contours) while no localization (blue contours) characterizes Ca. This points to its cationic character. The blue spots between the chemical species feature insulating systems, i.e. in metallic ones the interatomic space is of free-electron like with green contours (cf. Ref. [18], Fig. 2). The contours around O2 atoms exhibit a strong localization while being somehow isolated from the UO2-like entities. This illustrates the effect of the shorter U–O1 separation *versus* U–O2, letting suggest a stronger U–O1 bonding *versus* U–O2 one. This is further illustrated in the all electron calculations below.

3.4. Search for equilibrium parameters

Despite the relative agreement of the relaxed structure with experimental input parameters, a more reliable verification of the

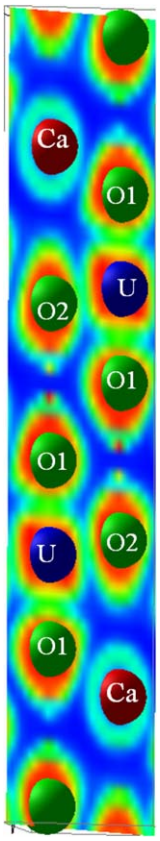

Fig. 2. (Color online) $CaUO_4$: electron localization function map along hexagonal *c*-axis.

ground state properties is better achieved from the energy *versus* volume (*E*,*V*) curves around the minima. These should have a quadratic variation and the *E*,*V* curves can be fitted using an equation of state (EOS) such as that provided by Birch [26]

$$E(V) = E(V_o) + \frac{9}{8}V_oB_o\left[\left(\frac{V_o}{V}\right)^{2/3} - 1\right]^2 + \frac{9}{16}B_o(B' - 4)V_o\left[\left(\frac{V_o}{V}\right)^{2/3} - 1\right]^3.$$

E_o, V_o, B_o and B' are the equilibrium energy, volume, bulk modulus and its pressure derivative, respectively. The Birch EOS is normally employed by assuming the following trend: the larger the value of B_o, the harder is the material. Beside isotropic compression we hypothesize a compression along the *c*-axis (cf. Fig. 1) within both the uranate and the fluorite. This anisotropic compression is meant to address the role of the linear O–U–O entity in comparison with fluorite. We note that this procedure applied for high structural anisotropy systems such as hexagonal graphite and BN, is experimentally used in establishing the EOS of less anisotropic systems such as Al_4C_3 [27]. The resulting energy *versus* volume curves are shown in Fig. 3. A difference appears for the uranate which shows for the anisotropic compression a strong variation of the energy around equilibrium while this feature is nearly absent for rh-Ca_2F_4 and both curves run similarly. This points to less compressibility of the uranate along the *c*-axis, likely due to the O–U–O linear polycation, while there should be little changes of the bulk moduli in fluorite, CaF_2. This is confirmed from the sets of fit equilibrium values shown in the inserts of the figures for the energy, the bulk modulus (B_o) and the volume (V_0). The latter is found in good agreement with

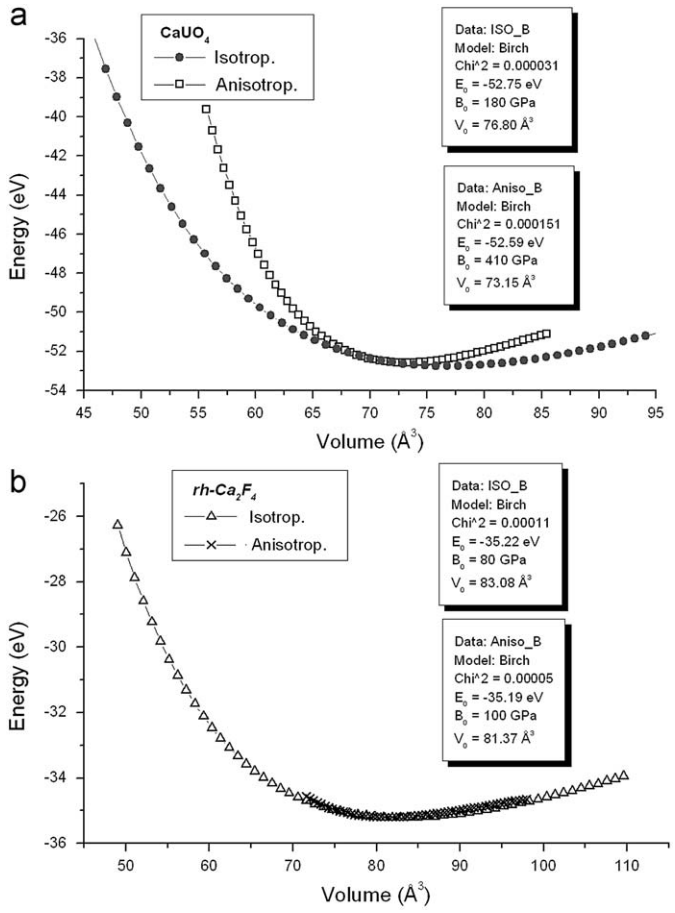

Fig. 3. Energy *versus* volume curves for isotropic and anisotropic compression along *c* hexagonal axis and equilibrium results from Birch EOS for rhombohedral systems: $CaUO_4$ (a) and Ca_2F_4 (b).

experiment although the equilibrium volume for rh-Ca2F_4 is slightly larger than experimental and geometry optimized values (Table 1). Nevertheless we want to discuss the magnitudes of the bulk moduli as an issue for the calculations: $B_o^{iso} = 80$ GPa is close to the Young modulus of 76 GPa of CaF_2 mineral. An anisotropic compression gives a slightly larger $B_o^{aniso} = 100$ GPa which could be related to the shorter apical Ca–F distance as found from the calculations. This means that for an ideal system with equal Ca–F distances there should be no difference between the two kinds of compressions. On the contrary there is a large discrepancy for the uranate between $B_o^{iso} = 180$ GPa which comes close to that known for UO_2 [8] on one hand and $B_o^{aniso} = 410$ GPa on the other hand. These magnitudes of B_o^{iso} and B_o^{aniso} agree with those of recently investigated $CdUO_4$ for which $B_o^{iso} = 166$ and $B_{aniso}^{b} = 423$ GPa; O–U–O linear group being along the orthorhombic *b*-axis of the cadmium uranate [28]. Then the difference arises from the short U–O apical distance. This was observed for UO_2F_2 where the very short U–O distance of ~1.74 Å [2] causes the large magnitude of $B_o^{aniso} = 590$ GPa [10]. Note that for the latter $B_o^{iso} = 150$ GPa is smaller than the one found for the uranate. This can be interpreted as follows: the relatively small magnitude of isotropic B_o for UO_2F_2 arises from the ease of gliding UO_2F_6 motifs along *x*, *y* directions while the insertion of Ca, which binds with oxygen (mainly O2) into the Van der Waals voids in the uranate hinders such an effect. Lastly we point out that for the pressure derivatives of the bulk modulus $B_{iso}' = 4$ and B_{aniso}'~9. Whereas the first value is the magnitude usually obtained, the anisotropic B' indicates an enhanced stiffness of the system [29,30].

4. All-electron calculations

At self-consistency a large charge transfer of ~3.5 electrons is observed from uranium towards the other species as well as to the ES. This expected trend is not exhibiting an ionic character such as U^{6+} and O^{2-}, rarely observed in the framework of the calculations. However the ionic/covalent features will be indirectly seen from the band structure, density of states as well as the chemical bonding analyzes.

4.1. Electronic band structure and orbital characters

The band structure and the corresponding trigonal Brillouin zone (BZ) are given in Figs. 4a and c. Energy reference along the *y*-axis is with respect to the top of the valence band (VB), E_V. At low energy O(2*s*) states are found, each forming two bands. The major feature is a band gap of ~3 eV leading to assign a semiconducting character to the oxide. In such a localized and strongly correlated 5*f* electrons system, we have further checked the impact of enhancing the correlation by GGA + U calculations using U = 4.5 and J = 0.5 eV used by Freyss et al. for the study of UO_2 and its defect structure [31]. The resulting band structure exhibits the same general features as in Fig. 4a with the difference of the increase of the band gap by ~1 eV, i.e. leading to a more insulating system. The localization of the uranium f bands in the CB is also the same. This probably arises from the fact that the system is involved with empty *f* subshell of hexavalent uranium ([Rn]5f^0). Therefore, the theoretical treatment using a scalar-relativistic calculational scheme and GGA functional used here should stand correctly. If one considers the experimentally proposed color of yellowish powder crystals [3], that would correspond to $E_g \leq 3$ eV band gap, then the calculations are in agreement with this feature. However care should be taken when attempting such comparisons in as far as the color might also arise from the grain size and the state of crystallinity, so that this should only be taken as a qualitative statement. Considering the green luminescence of uranyl in CaF_2 as studied by Lupei and Lupei [32], the energy of this emission is ~2.5 eV as observed in the spectra of Fig. 1 of that paper. The U^{6+} ion can be considered with 5f^0 configuration and the optical transitions involved are of charge transfer type (ligand-to-metal charge transfer). In fact Lupei and Lupei excite U^{6+} in the U.V. at 350 nm (3.5 eV), certainly in the charge transfer band at higher energy than emission. This is consistent with the value of the band gap of ~3 eV, determined by calculations in our case, it can be suggested that exciting a p-electron from oxygen (top of the VB) to empty U(5*f*) bottom of CB, would lead to creating a discrete 5f^1 level in the CB and unstable single-charged oxygen (O^{-1}) because of its charge transfer state. Then the system relaxes with returning of the electron back on oxygen, leading to the green emission.

There is little dispersion of the bands which is a characteristics of insulating systems as it can be observed from Fig. 4b of rh-Ca_2F_4. Furthermore there is a flat band behavior mostly pronounced for the *Z*–*Γ* direction, i.e., along k_z direction as shown in Fig. 4c of the BZ. This corresponds to the *Γ*-*A* direction in the hexagonal BZ and describes the passage from band dispersions in (k_x, k_y) plane to another along k_z. From a crystal field analysis of the f states the band at the top of the VB (HOMO, highest occupied molecular orbital, in molecular chemistry language) is found to be f_{z^3} type, i.e. with pure z-components, aligned along the *c*-axis, together with a presence of oxygen p-bands. This shows the involvement of U(f) states in the bonding close to E_V, top of the VB although the 7 bands relevant to uranium *f* sub-shell are mainly found at ~4 eV with CB. The corresponding LUMO (lowest unoccupied molecular orbital) at the bottom of the CB is found to be of $f_{x,y}$ character. The dispersive bands at the top of the CB correspond to antibonding states. There are 12 bands in the narrow energy window of the VB top, corresponding to

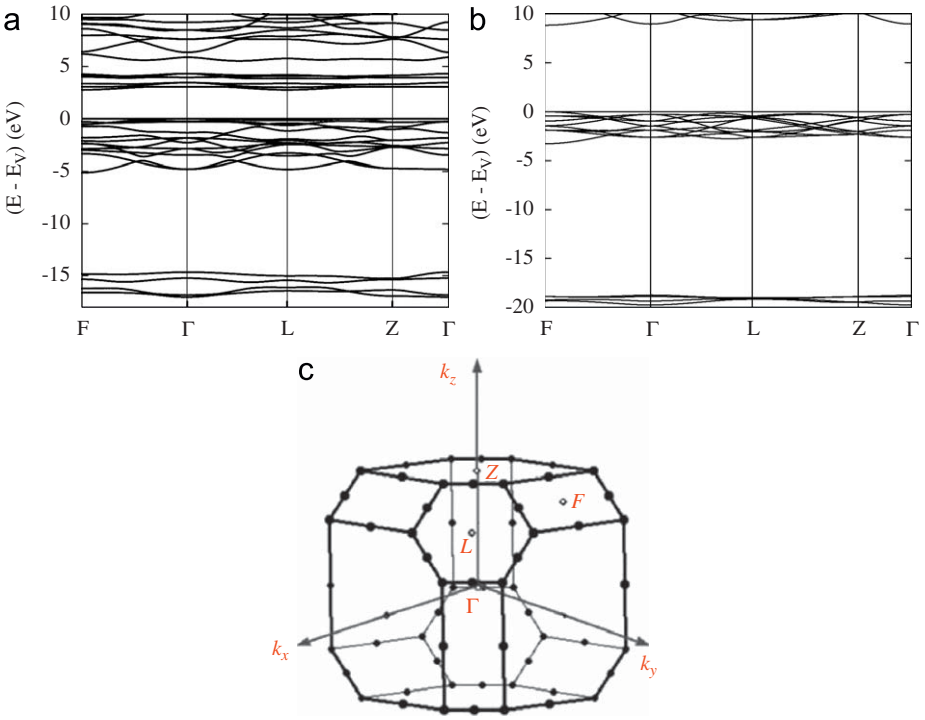

Fig. 4. Electronic band structure of $CaUO_4$ (a), Ca_2F_4 (b) and the rhombohedral primitive Brillouin zone with remarkable points: zone center Γ and dispersion points F, L and Z (c).

oxygen p-like states mixing with U itinerant (delocalized) states. Adding the four *s*-like bands at ~ -15 eV, one has 16 bands in the VB. With each one containing 2 electrons, there are 32 electrons corresponding to the valence electron count of the chemical system: one U ($7s^2$, $6d^1$, $5f^3$) , one Ca ($4s^2$) and four O ($2s^2$, $2p^4$). The oxide system is isoelectronic of UO_2F_2 and Ca_2F_4; it is expected that ionic character increases in the series. We further illustrate this behavior by the plot of the band structure of rh-Ca_2F_4 (Table 1) in Fig. 4b. While the band count of 16 is the same in the VB with F(2*s*) band lying at lower energy (~ -20 eV) than O(2*s*), the bands are much less dispersed and the gap is larger.

The role of uranium itinerant/localized states and the respective roles played by oxygen at sites O1 and O2, can be better observed by weighting the bands with orbital characters. The resulting so-called *fat* bands are shown in Fig. 5. From Figs. 5a and b, the *f* character is dominant within the CB as well as at the top of the VB while the *d* character dominates the lower part of the VB as well as the lower energy four bands indicating a quantum mixing between O(2*s*) and U(*d*). From the fat bands showing the *p* characters of oxygen at O1 and O2 sites, (Figs. 5c and d), these are found dominant respectively at the top and bottom of the VB. The absence of dispersion along the Z–Γ direction can be mainly assigned to bands weighted with O2 states in the lower part of the VB. The dispersive bands at the top of the CB correspond to antibonding states as it will be confirmed from the chemical bonding analysis in next section. From the fat bands of Figs. 4a and b they have U(*f*) character for the lower part and U(*d*) character for the upper part.

4.2. Band structures of modified hexavalent uranate, introducing U^{5+}

The substoichiometry in $CaUO_4$ was observed by different authors [33,34] leading to reduced oxide systems. This involves the formation of pentavalent uranium which has one f electron, i.e., [Rn]$5f^1$ instead of the [Rn]$5f^0$ configuration of hexavalent uranium of pristine oxide. The partial occupation of uranium 5*f* subshell leads to the lowering of the f band toward the top of the valence band. In order to show the resulting band structure, complementary band calculations were done with an 8-f.u. supercell ($Ca_8U_8O_{32}$) in which two oxygen out of the 32 were removed and replaced by empty spheres, ES, (cf. Section 2). The resulting band structure given in Fig. 6a shows almost the same shape as that of the 1 f.u. $CaUO_4$ (Fig. 4) with a shift of f states toward the zero energy (now labeled E_F) and a reduced gap of less than 2 eV. This is also confirmed for the band structure of a hypothetic $ScUO_4$ system where the trivalent scandium replacing divalent calcium leads to the pentavalent uranium. The band structure is shown in Fig. 6b which exhibits similar features to former graphs. Lastly the presence of pentavalent uranium in oxides was recently investigated in $NaUO_3$ by neutron diffraction. It reveals ordered magnetic moment on U and a long range antiferromagnetic order [35].

4.3. Density of states and chemical bonding

The band features can be further discussed using the site projected density of states (PDOS) and the chemical bonding properties. This is given in Fig. 7. In all plots the zero energy along the *x*-axis is at the top of the VB. The PDOS show that at lowest energy O(2*s*)-like PDOS are identified with a larger localization for O1 (two peaks) than O2 which show some dispersion. This is likely due to the mixing of O2 with Ca which has *s*-like orbitals and to their reduced mixing with uranium due to the larger U–O2 separation. The Ca PDOS are of low intensity and extend all over the VB. The ES PDOS which have similar valence basis set to atomic constituents are shown to extend throughout the VB as well as the CB with small magnitude. This means that they have ensured for the continuity of the charge density within such an open structure system. In the energy window $[-5, E_V]$ oxygen character is found dominating for both O1 and O2. Despite some

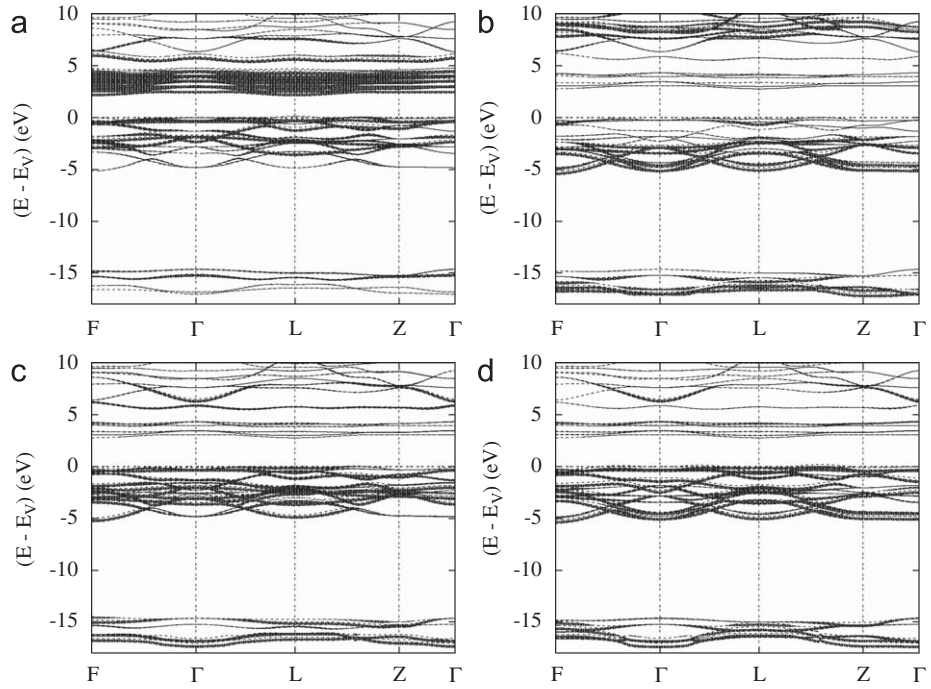

Fig. 5. Band structure of $CaUO_4$ with orbital characters: (a) U(f)-weighted, (b) U(d)-weighted, (c) O1-weighted and (d) O2-weighted.

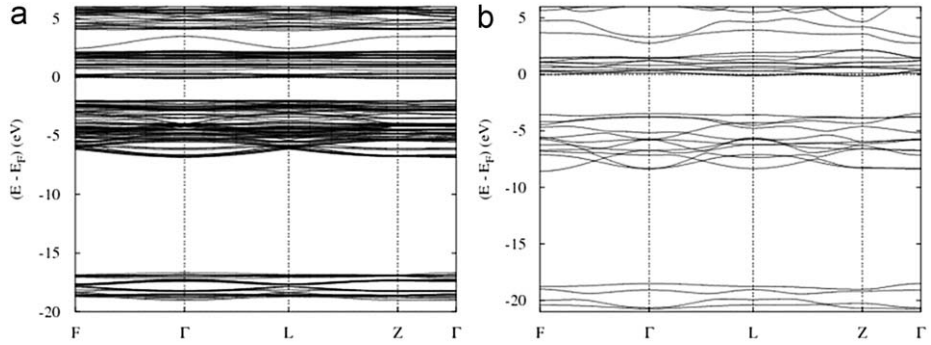

Fig. 6. Band structures of modified hexavalent uranate, introducing U^{5+}: (a) $Ca_8U_8O_{30}\diamond_2$ supercell ($\diamond$ represents oxygen vacancies); (b) hypothetic $ScUO_4$.

intensity differences their PDOS run similarly thus pointing to quantum mixing between constituents' valence basis sets. However some differences for U–O bonding between O1 and O2 sites should be traced out from a qualitative analysis of the chemical bonding. This is discussed in Fig. 7b exhibiting the ECOV which show a bonding behavior throughout the VB with larger bonding intensity for U–O1 *versus* U–O2 at −15 eV for the bonding with O(2*s*) and in the energy window, $[-5\,\text{eV}, E_V]$. It is interesting to note the more prevailing O2 bonding at the lower part of this energy window, which complies with a more ionic character. The *s*-like Ca–O bonding is of very low intensity and it is not shown in the plots. The relative strength of bonding can be better estimated from the integrated ECOV, *i* ECOV, then the larger the area, the stronger the bonding is. This is shown in Fig. 7c. The U–O1 bond has a larger area and is found stronger than U–O2. This follows from the shorter distances U–O1 *versus* U–O2. However this is not as sharp a difference as in uranyl fluoride where both the aspects of the electronegativity change between O and F and the larger difference of U–F/U–O distances add up to give its physico-chemical characteristics [10].

5. Conclusion

In this work original results based on DFT on $CaUO_4$, isostructural with uranyl fluoride and rhombohedral fluorite (rh-Ca_2F_4) have been presented and discussed comparatively. Complementary computations with pseudo-potential and all electron methods were carried out with the objectives of providing consistent data for the equation of state and energy derived quantities on one hand and a detailed study of the electronic band structure characteristics on the other hand. It has been mainly shown that the oxide system, contrary to rh-Ca_2F_4, shows different responses to isotropic *versus* anisotropic volume changes leading to assign this feature to the incompression of the O–U–O linear entity. It is characterized as a semiconductor with a valence band dominated by oxygen which behaves both as covalent and ionic according to its distance to U and Ca. The emerging picture is that the linear uranyl polycation UO_2^{2+} would have 'different sizes' according to its chemical surrounding with more (ex. in F in UO_2F_2) of less (ex. O in $CaUO_4$) ionic environments. The elaboration of single crystals for $CaUO_4$ would

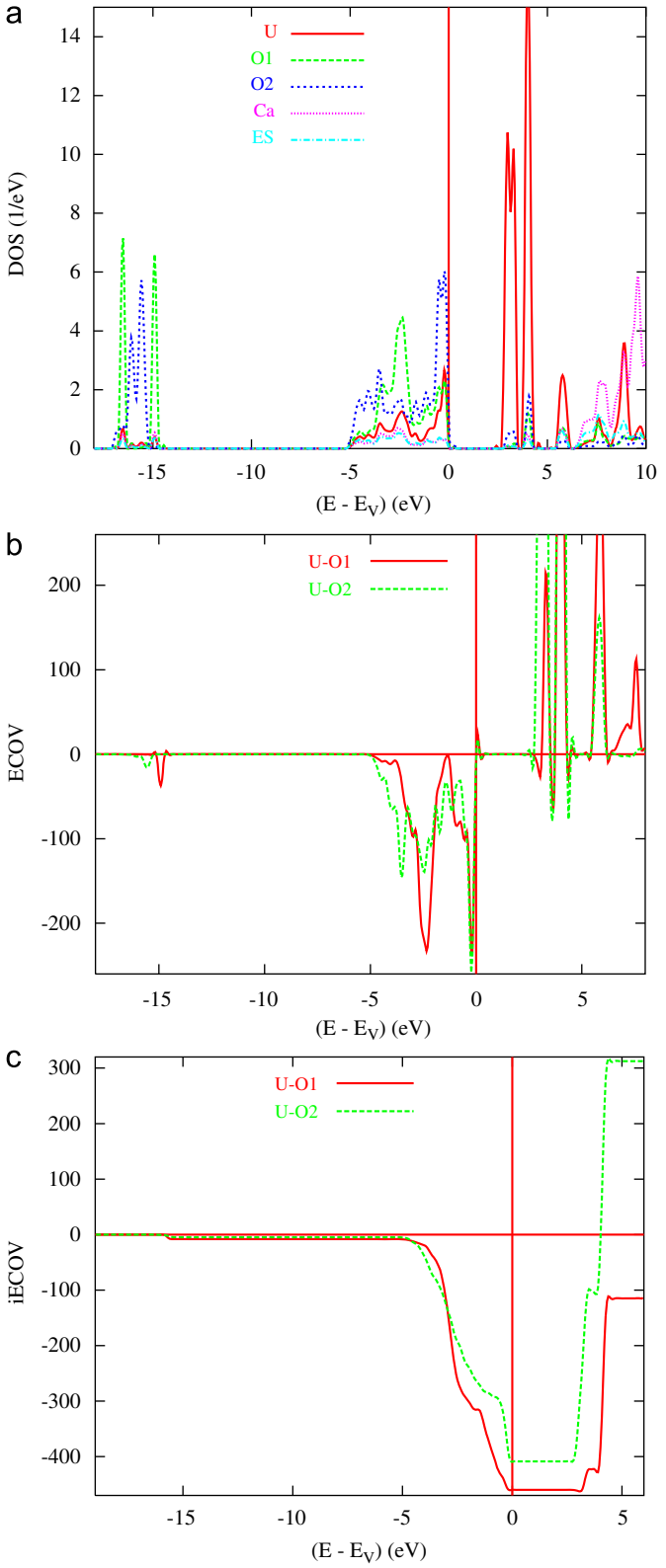

Fig. 7. (Color online) Rhombohedral $CaUO_4$: site projected density of states (a), chemical bonding from ECOV (b) and relative bond strengths for U–O1 and U–O2 (areas underneath peaks) and from integrated ECOV (c).

allow to verify the anisotropy of the mechanical compression through, in particular, micro-indentation tests. Such a system can be considered as an illustration of a structure where a strong anisotropy of the U–O chemical bonds induces at the macro-scale an anisotropy of the physical properties.

Acknowledgments

Computational facilities were provided by the supercomputers of the University Bordeaux 1 within the M3PEC Mésocentre Régional (http://www.m3pec.u-bordeaux1.fr). Discussions with Dr Alain Garcia, Optics group of ICMCB-CNRS, are gratefully acknowledged.

References

[1] W.H. Zachariasen, Acta Cryst. 1 (1948) 265.
[2] M. Atoji, M.J. McDermott, Acta Cryst. B 26 (1970) 1540.
[3] W.H. Zachariasen, Acta Cryst. 1 (1948) 281.
[4] S. Ostanin, P. Zeller, Phys. Rev. B 75 (2007) 073101.
[5] P. Hohenberg, W. Kohn, Phys. Rev. 136 (1964) 864.
[6] W. Kohn, L.J. Sham, Phys. Rev. 140 (1965) 1133.
[7] L.E. Roy, T. Durakiewicz, R.L. Martin, J.E. Peralta, G.E. Scuseria, C.G. Olson, J.J. Joyce, E. Guziewicz, J. Comput. Chem. 29 (2008) 2288.
[8] H.Y. Geng, Y. Chen, Y. Kaneta, M. Kinoshita, Phys. Rev. B 75 (2007) 054111.
[9] R.A. Evarestov, A.I. Panin, A.V. Bandura, Russ. J. Gen. Chem. 78 (2008) 1823.
[10] S.F. Matar, Solid State Sci. 11 (2009) 1380–1385.
[11] G. Kresse, J. Furthmüller, Phys. Rev. B 54 (1996) 11169.
[12] P.E. Blöchl, Phys. Rev. B 50 (1994) 17953.
[13] G. Kresse, J. Joubert, Phys. Rev. B 59 (1999) 1758.
[14] D.M. Ceperley, B.J. Alder, Phys. Rev. Lett. 45 (1980) 566.
[15] J. Perdew, K. Burke, M. Ernzerhof, Phys. Rev. Lett. 77 (1996) 3865.
[16] H.J. Monkhorst, J.D. Pack, Phys. Rev. B 13 (1976) 5188.
[17] A.D. Becke, K.E. Edgecombe, J. Chem. Phys. 92 (1990) 5397.
[18] S.F. Matar, Solid State Sci. 11 (2009) 894.
[19] A.R. Williams, J. Kübler, C.D. Gelatt, Phys. Rev. B 19 (1979) 6094.
[20] V. Eyert, The augmented spherical wave method—a comprehensive treatment, in: Lecture Notes in Physics, Springer, Berlin, Heidelberg, vol. 719, 2007.
[21] V. Eyert, K.-H. Höck, Phys. Rev. B 57 (1998) 12727.
[22] V. Eyert, J. Comput. Phys. 124 (1996) 271.
[23] G. Bester, M. Fähnle, J. Phys. Condens. Matter 13 (2001) 11541.
[24] R. Hoffmann, Angew. Chem. Int. Ed. Engl. 26 (1987) 846.
[25] R. Dronskowski, P.E. Blöchl, J. Phys. Chem. 97 (1993) 8617.
[26] F. Birch, J. Geophys. Res. 83 (1978) 1257.
[27] V.L. Solozhenko, O.O. Kurakevych, Solid State Commun. 133 (2005) 385.
[28] S.F. Matar, Chem. Phys. Lett. 476 (2009) 213.
[29] S. Raju, E. Mohandas, V.S. Raghunathan, J. Phys. Chem. Solids 58 (1997) 1367.
[30] M. Mattesini, S.F. Matar, Phys. Rev. B 65 (2002) 075110.
[31] M. Freyss, J. Durinck, B. Dorado, Colloque 3M, Saclay, 2–3 June 1008, France, unpublished.
[32] A. Lupei, V. Lupei, J. Phys. C Solid state Phys. 12 (1979) 1123.
[33] A. Prodan, F.W. Boswell, Acta Cryst. B 42 (2) (1986) 141.
[34] K. Takahashi, T. Fujino, L.R. Morss, J. Solid State Chem. 105 (1993) 234.
[35] S. Van den Berghe, A. Leenaers, C. Ritter, J. Solid State Chem. 177 (2004) 2231.